



## Targeting infected host cells *in vivo* via responsive azido-sugar mediated metabolic cell labeling followed by click reaction



Yang Bo<sup>a</sup>, Yunjiang Jiang<sup>a</sup>, Kangmei Chen<sup>c</sup>, Kaimin Cai<sup>a</sup>, Wenming Li<sup>a</sup>, Jarron Roy<sup>b</sup>, Yan Bao<sup>c,a,\*</sup>, Jianjun Cheng<sup>a,b,\*</sup>

<sup>a</sup> Department of Materials Science and Engineering, University of Illinois at Urbana-Champaign, Urbana, IL, 61801, United States

<sup>b</sup> Department of Bioengineering, University of Illinois at Urbana-Champaign, Urbana, IL, 61801, United States

<sup>c</sup> Medical Research Center, Sun Yat-Sen Memorial Hospital, Sun Yat-Sen University, Guangzhou, Guangdong, 510120, PR China

### ARTICLE INFO

#### Keywords:

Infection targeting  
Cell labeling  
Click chemistry  
Drug design  
Sugar

### ABSTRACT

The early *in vivo* diagnosis of infectious disease foci is largely hindered by invasion and concealment of pathogens in host cells, making it difficult for conventional probes to detect and analyze intracellular pathogens. Taking advantage of the excessively produced reactive oxygen species (ROS) within host cells, herein we report the design of thiol-hemiketal blocked N-azidoacetyl galactosamine (Ac<sub>3</sub>GalNAzSP), an azido unnatural sugar bearing an unprecedented designed ROS-responsive moiety for targeted labelling of infected host cells. Ac<sub>3</sub>GalNAzSP showed great stability under physiological conditions, specifically released active unnatural sugar in host cells overproducing ROS, metabolically labeled infected host cells with azido groups, and enabled targeting *in vivo* infection sites by subsequent Click Chemistry reactions, substantiating an unprecedented approach for targeting infected host cells. This technique could be a powerful tool for early *in vivo* diagnosis and targeted treatment of infectious disease.

### 1. Introduction

Bacterial infections present an outstanding clinical threat despite the availability of antibiotic treatments. If not effectively treated at early stages, bacterial infections may lead to irreversible pathological transformations towards high-burden settings and severe or lethal diseases such as sepsis [1], tuberculosis [2], salmonellosis [3], or other widespread pathogenic transmissions [4]. An efficient, rapid method to detect early-stage infectious disease foci *in vivo* with high accuracy and sensitivity is therefore crucial. Tissue biopsy and culture are current clinical procedures for the diagnosis of most infectious pathogens. These processes, however, may take days to complete, during which the infection may transform, spread, and become systemic with high bacterial burdens [5,6] and render treatment very challenging. There have been attempts to utilize pathogen-specific ligands coupled with fluorescent probes for the non-invasive optical detection of infectious foci [7–11], especially for extracellular pathogens exposed at the infection site. However, many pathogens invade and survive inside mammalian cells upon being engulfed by phagocytic cells responsible for bacterial clearance, making it very challenging to detect internalized pathogens *in vivo* with conventional probes due to their poor cell penetration

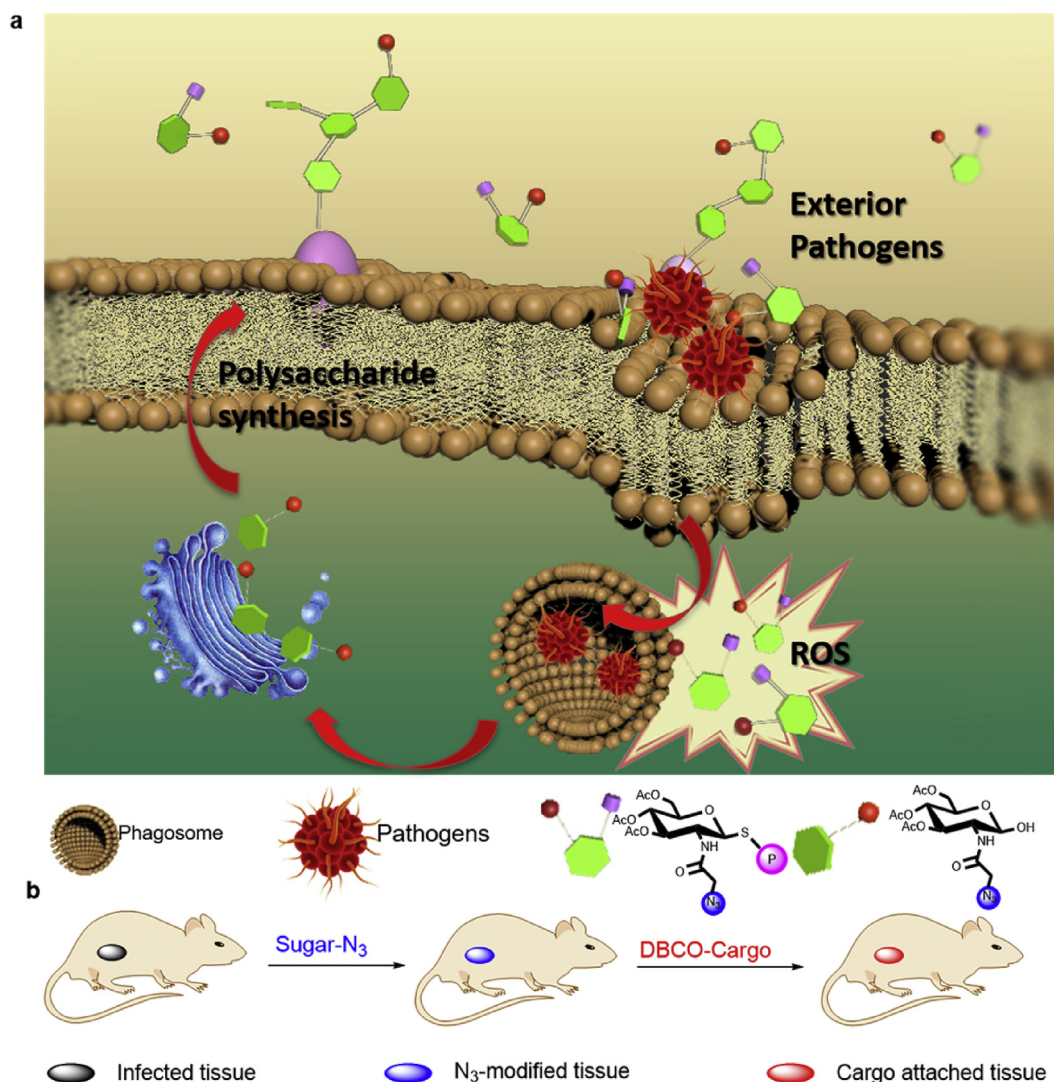
capability [12]. For instance, *S. aureus* is taken up by host phagocytic cells, primarily neutrophils and macrophages, within minutes after systemic infection [13–16]. Once uptaken in the blood-borne phagocytic cells, *S. aureus* is shielded from diagnosis and antibiotic treatment. These infected host cells subsequently act as ‘Trojan horses’ for the systemic dissemination of bacteria. Therefore, there is an urgent clinical need to develop non-invasive targeting techniques that can readily identify a broad-spectrum of pathogens in host cells and provide a sensitive readout of disease burden at early stages of infection.

To introduce biorthogonal functional groups to glycoproteins on cell surfaces, metabolic labelling with unnatural sugars has been widely used for glycan visualization, glycoproteome mapping, and cell labelling [17–20]. Small molecule metabolic azido-sugars can mediate tissue specific imaging and delivery via a trigger-responsive design, which converts a cell-specific intracellular signal into targetable artificial antigens on cell surfaces [21–25]. This strategy has obvious advantages over antibodies for disease targeting because azido-sugars enable more efficient tissue penetration and cellular uptake, transforming non-targetable intracellular signals to targetable groups on the tissue surface at a density orders of magnitude higher than typical antigens. This facilitates an effective targeting mechanism via highly efficient *in vivo* Click

\* Corresponding author. Department of Materials Science and Engineering, University of Illinois at Urbana-Champaign, Urbana, IL, 61801, United States.

\*\* Corresponding author. Medical Research Center, Sun Yat-Sen Memorial Hospital, Sun Yat-Sen University, Guangzhou, Guangdong, 510120, PR China.

E-mail addresses: [baoy5@mail.sysu.edu.cn](mailto:baoy5@mail.sysu.edu.cn) (Y. Bao), [jianjunc@illinois.edu](mailto:jianjunc@illinois.edu) (J. Cheng).



**Scheme 1.** a) Reactive oxygen species (ROS) responsive release of synthetic 1'-modified azido-galactosamine and subsequent labelling of infected host cell via intrinsic metabolic machine. b) *In vivo* selective labelling of infectious foci with azido groups and subsequent infection targeting via click chemistry.

chemistry post metabolic labelling [21,26]. Those properties make unnatural sugar mediated labelling a more viable strategy for targeting infected host cells.

Reactive oxygen species (ROS), generated by immune cells (e.g., macrophages and neutrophils) to facilitate host defense responses towards intracellular pathogens, are released immediately upon infection by both Gram-negative or Gram-positive bacteria [27]. The intracellular ROS concentration in host cells may increase by 10–100 fold [8], making ROS a viable trigger to achieve highly specific targeting. Herein, we report an unprecedented design of unnatural azido-sugars that can selectively label infected host cells through a ROS specific mechanism both *in vitro* and *in vivo*, presenting azido groups on the surface of the infected host cells for further copper-free click chemistry mediated cargo delivery to infected cells (Scheme 1).

## 2. Methods

### 2.1. HPLC quantification of Ac<sub>3</sub>GalNAzSP under H<sub>2</sub>O<sub>2</sub> environment

Ac<sub>3</sub>GalNAzSP (1 mg/mL) was dissolved in PBS (1 mL, add 1% Tween - 80) and H<sub>2</sub>O<sub>2</sub> stock solution (30% H<sub>2</sub>O<sub>2</sub> by weight) was added to obtain the final concentration of 10 mM H<sub>2</sub>O<sub>2</sub>. The mixture was incubated at 37 °C. At assigned time data points, 25 μL aliquot of the

mixture was added to 500 μL 1:1 Acetonitrile and 0.1% TFA water mixed solvent and quenched by addition of sodium pyruvate solution (50 μL, 250 mM). DBCO-Cy5 (7 μL in DMSO, 10 mM) was added and the solution was incubated overnight. The HPLC traces were collected with a PDA detector at 254 nm (for quantification of structures with aromatic domain) and fluorescence detector with excitation at 650 nm and emission at 688 nm (for quantification of species with reactive azide groups). Each starting material and final compound was quantified to standard curves generated from pure compounds.

### 2.2. Stability of MBTAAG in physiological conditions

MBTAAG (1 mg/mL) was diluted with PBS or DMEM cell medium supplied with 10% (v/v) FBS. The mixture was incubated at 37 °C. At assigned time data points, 25 μL aliquot of the mixture was added to 500 μL 1:1 Acetonitrile and 0.1% TFA water mixed solvent. The HPLC trace was collected with a PDA detector at 254 nm (for quantification of structures with aromatic domain). Each starting material and final compound was quantified to the standard curve generated from pure compounds.

### 2.3. Confocal imaging of azido-sugar labeled proinflammatory cells

RAW264.7 cells were seeded onto coverslips in a 6-well plate at a density of  $5 \times 10^4$  cells per well for 12 h. Azido sugar MBTAAG or AAG (50  $\mu\text{M}$ ) was added and the cells were incubated at 37 °C for 48 h, followed by addition of 5  $\mu\text{g}/\text{mL}$  LPS (For ROS inhibition group, LPS was spiked with 5 mM TEMPOL for inhibition of ROS production), and cells were incubated for another 12 h. After washing with PBS, cells were incubated with DBCO-Cy5 (20  $\mu\text{M}$ ) for 1 h and fixed with 4% paraformaldehyde (PFA) solution, followed by staining of cell nuclei with Hoechst 33342 (10  $\mu\text{g}/\text{mL}$ ). The coverslips were mounted onto microscope slides and imaged under a confocal laser scanning microscope.

### 2.4. Flow cytometry analysis of azido-sugar labeled proinflammatory cells

RAW264.7 cells were seeded in a 6-well plate at a density of  $5 \times 10^4$  cells per well for 12 h. Azido sugar MBTAAG or AAG (50  $\mu\text{M}$ ) was added and the cells were incubated at 37 °C for 48 h, followed by addition of 5  $\mu\text{g}/\text{mL}$  LPS (For ROS inhibition group, LPS was spiked with 5 mM TEMPOL for inhibition of ROS generation), and the cells were incubated for another 12 h. After washing with PBS, cells were incubated with DBCO-Cy5 (20  $\mu\text{M}$ ) at 37 °C for 1 h and the free DBCO-Cy5 were washed away with PBS. Cells were lifted by incubating with trypsin solution and analyzed by flow cytometry.

### 2.5. Western blotting analysis of azido-sugar labeled pro-inflammatory cells

RAW264.7 cells were seeded in a 6-well plate at a density of  $1 \times 10^5$  cells per well for 12 h. Azido sugar MBTAAG or AAG (50  $\mu\text{M}$  in DMSO) was added and the cells were incubated at 37 °C for 48 h, followed by addition of LPS (5  $\mu\text{g}/\text{mL}$  in PBS), the cells were incubated for another 12 h. After washing with PBS, cells were lysed with lysis buffer (50 mM Tris-HCl, 1% SDS, pH 7.4), and the lysate was incubated at 4 °C for 30 min. Following the removal of the lysate debris by centrifugation at 10000 rpm, the protein concentration of cell lysate was quantified by using standard BCA assay. After adjusting the amount of protein, iodoacetamide solution (60 mM, 1  $\mu\text{L}$  in 20  $\mu\text{L}$  lysate) was added and incubated at 37 °C for 1 h to fully block the free thiol groups in proteome. DBCO-(PEG)<sub>4</sub>-biotin (10 mM, 1  $\mu\text{L}$  in 20  $\mu\text{L}$  lysate) was added to the mixture and the resulting mixture was incubated overnight at 37 °C. The protein mixture labeled with biotin was mixed with 2  $\times$  sample buffer, heated for 10 min at 95 °C and subjected to electrophoresis. After standard membrane transfer, the membrane was incubated with streptavidin-HRP at room temperature for 1 h and washed with 1  $\times$  TBST at room temperature while shaking for 10 min. The blots were developed with ECL Western Blotting substrate and the membrane was exposed and imaged.

### 2.6. MBTAAG labelling of in vitro pathogen infected macrophage

**Confirmation of intracellular ROS generation in infected macrophages with confocal fluorescence microscopy.** RAW264.7 cells ( $5 \times 10^4$  cells/well in a 6-well plate) were seeded and incubated. MBTAAG or AAG (50  $\mu\text{M}$  in DMSO) was added and the cells were incubated at 37 °C for 48 h. After that, *E. Coli* or *B. Subtilis* was added to each well with MOI = 5 (bacteria per cell). The bacteria were co-incubated with the cells for 1 h, washed with PBS (2  $\times$  1 mL) to remove extracellular bacteria, 1 mL DMEM medium (containing 50  $\mu\text{M}$  the abovementioned sugar precursor) spiked with 2  $\mu\text{g}/\text{mL}$  gentamycin was added for 12 h at 37 °C, and DCFDA solution in DMSO was added to the medium to obtain final concentration of 10  $\mu\text{M}$ . After washing with PBS, the cells were incubated with DBCO-Cy5 (20  $\mu\text{M}$  in PBS) for 1 h and fixed with 4% paraformaldehyde (PFA) solution, followed by staining of cell nuclei with Hoechst 33342 (10  $\mu\text{g}/\text{mL}$ ). The coverslips were mounted onto microscope slides and imaged under a confocal laser scanning

microscope.

**Flow cytometry analysis.** RAW264.7 cells were seeded in a 6-well plate at a density of  $5 \times 10^4$  cells per well for 12 h. Azido sugar MBTAAG or AAG (50  $\mu\text{M}$ ) was added and the cells were incubated at 37 °C for 48 h. After that, GFP expressing *E. Coli* or *B. Subtilis* was added to each well with MOI = 1, 5, 10, 25, 100 (bacteria per cell). The bacteria were co-incubated with the cells for 1 h and washed with PBS (2  $\times$  1 mL) to remove the extracellular bacteria. DMEM medium (contain 50  $\mu\text{M}$  above sugar precursor) spiked 2  $\mu\text{g}/\text{mL}$  gentamycin was added. The cells were incubated for 12 h at 37 °C. After washing with PBS, cells were incubated with DBCO-Cy5 (20  $\mu\text{M}$  in PBS) at 37 °C for 1 h and the free DBCO-Cy5 were washed away with PBS. Cells were lifted by incubating with trypsin solution and analyzed by flow cytometry.

### 2.7. In vivo pathogen infected myositis site specific labeling of MBTAAG and biodistribution

Female BALB/c mice (8 weeks) were anaesthetized with isoflurane and the hair on the thigh and back was removed. A suspension of *E. coli* ( $10^6$  CFUs) in saline (50  $\mu\text{L}$ ) was injected into the left rear thigh muscle (injection depth 5 mm). Saline (50  $\mu\text{L}$ ) was injected into right rear thigh muscle as the negative control (injection depth 5 mm). The mice were divided into three groups: PBS + DBCO-Cy5 (Group 1), MBTAAG + DBCO-Cy5 (Group 2), AAG + DBCO-Cy5 (Group 3). After 12 h the mice were injected with MBTAAG (76.8 mg/kg in 200  $\mu\text{L}$  PBS) (group 1) through the tail vein injection, injection of PBS (group 2) or AAG (64.0 mg/kg in 200  $\mu\text{L}$  PBS) (group 3) were used as controls. After 12 h post injection of MBTAAG, DBCO-Cy5 (5 mg/kg in 200  $\mu\text{L}$  PBS) was intravenously injected and its biodistribution was monitored by using the Bruker In Vivo Xtreme Imaging System with a 630 nm (excitation)/700 nm (emission) filter at 2, 4, 8, and 12 h post injection of DBCO-Cy5, respectively. The collected images were analyzed and the fluorescent intensity of Region of Interest (ROI) was quantified using Bruker molecular imaging software. At 12 h post injection of DBCO-Cy5, infected thigh and uninfected thigh, heart, liver, spleen, lung, kidneys were harvested from mice and imaged *ex vivo*. *Ex vivo* images were quantified by measuring fluorescence intensity at selected ROIs. For the MBTAAG labeling biodistribution analysis, at 12 h post the injection of MBTAAG, infected muscle and organs were harvested for western blotting analyses following the above-mentioned procedures.

### 2.8. Confocal imaging of infected tissue

After *ex vivo* imaging, thighs were directly frozen in O.C.T. compound, bisected with a thickness of 8  $\mu\text{m}$  on a cryostat (Leica CM3050S), and stained with Hoechst 33342 (2  $\mu\text{g}/\text{mL}$ ) and Rb pAb to CD68 coupled with Alexa Fluorophore 555 conjugated Goat pAb to Rb IgG for macrophage population immunostaining. After multiple washing steps, coverslips were mounted onto the microscope slides with the addition of ProLong Gold antifade reagent, and the prepared samples were stored in the dark for confocal imaging.

### 2.9. In vivo labeling specificity test by ROS chemiluminescent imaging

Female BALB/c mice (8 weeks) were anaesthetized with isoflurane and the hair on the thigh and back was removed. A suspension of *E. coli* ( $10^6$  CFUs) in saline (50  $\mu\text{L}$ ) was injected into the rear thigh muscle (injection depth 5 mm) at both flanks. 100 mg/kg TEMPOL was s.c. injected (injection volume 50  $\mu\text{L}$ ) 3 times into the right flank for the control at 6, 18, 30 h. For L-012 chemiluminescent imaging, 5 mg/kg in 50  $\mu\text{L}$  injection volume was used, 10 min post injection of L-012, bioluminescent imaging was conducted by the Bruker In Vivo Xtreme Imaging system with a CCD camera with a filter of 700 nm. After 12 h of infection, the mice were injected with MBTAAG (76.8 mg/kg in 200  $\mu\text{L}$  PBS) through tail vein injection while PBS injection was used as a

control. 12 h post injection of MBTAAG, DBCO-Cy5 (5 mg/kg in 200  $\mu$ L PBS) was intravenously injected and its biodistribution was monitored by using the Bruker In Vivo Xtreme Imaging System with a 630 nm (excitation)/700 nm (emission) filter at 12 h post injection of DBCO-Cy5.

### 2.10. Trypan blue cell toxicity assay

RAW264.7 cells were plated in a 24-well plate at a density of 500,000 cells/mL in full DMEM media supplemented with either 10  $\mu$ M or 50  $\mu$ M MBTAAG. At 24, 48, and 72 h, the cells were suspended with trypsin, and a 10  $\mu$ L sample was taken from each of the samples and mixed 1:1 with a 0.4% (w/v) trypan blue solution in PBS. Samples were incubated for 1 min at room temperature before being loaded onto a hemocytometer where live and dead cells were counted. Each sample was made in triplicate for each time point.

### 2.11. In vivo biocompatibility study

MBTAAG (76.8 mg/kg) was intravenously injected to 8-week-old ICR mice, mice with solvent injection were used as control ( $n = 5$  per group). At 48 h after administration, blood from each mouse was extracted for biochemical tests, and the heart, liver, spleen and kidneys were separated for H&E staining. Briefly, the levels of 4 serum biochemical parameters, including aspartate aminotransferase (ALT), aspartate aminotransferase (AST), blood urea nitrogen (BUN or UREA), creatinine (CREA), were evaluated with Hitachi 3100 Chemistry analyzer. The tissue samples were immediately fixed with 4% Paraformaldehyde (PFA), embedded in paraffin, sectioned at 4  $\mu$ m and stained with H&E. Characterization of all the collected target tissues for inflammatory cell infiltrate including macrophages and neutrophils was performed by systemic microscopic evaluation at 400  $\times$  magnification.

### 2.12. Blood compatibility hemolysis assay

The toxicity of MBTAAG was tested by its hemolytic activity against HRBCs following established protocols. Serial 2-fold dilution of MBTAAG with PBS buffer gives a range of predetermined concentrations. Fresh HRBC suspension (1 mL) was washed twice with PBS buffer (12 mL) and collected by centrifugation at 3000 rpm (1000  $\times$ g) before being re-dispersed in PBS buffer (15 mL) to reach a HRBC concentration of  $\sim$ 1.0% (v/v). Aliquots of this diluted HRBC suspension (160  $\mu$ L) were mixed with diluted MBTAAG solutions (40  $\mu$ L) in 1.5 mL micro-centrifugation tubes. The tubes were secured in a shaker incubator and shaken at 250 rpm at 37  $^{\circ}$ C for 60 min. PBS buffer (40  $\mu$ L) or Triton X-100 (40  $\mu$ L, 1% v/v) mixed with HRBC suspension (160  $\mu$ L) were used as negative and positive controls, respectively. The tubes were centrifuged at 3000 rpm (1000  $\times$ g) for 5 min to pellet the intact cells and cell fragments. Supernatant (30  $\mu$ L) of each test sample added into a 96-well plate with each well contains PBS buffer (100  $\mu$ L). The absorbance at 405 nm was measured with a microplate reader (PerkinElmer Victor<sup>3</sup> V). The percentage of hemolysis ( $\psi$ ) was calculated by:

$$\psi = \frac{OD_{405, \text{sample}} - OD_{405, \text{NC}}}{OD_{405, \text{PC}} - OD_{405, \text{NC}}} \times 100\%$$

where  $OD_{405, \text{sample}}$  is the absorbance of HRBC supernatant treated with a MBTAAG concentration.  $OD_{405, \text{PC}}$  and  $OD_{405, \text{NC}}$  are the absorbance of positive and negative control, respectively.  $HC_{50}$  is defined as the minimal sample concentration that causes 50% hemolysis, which is commonly regarded as the index of toxicity.

### 2.13. Statistical analysis

The statistical analysis was performed by one-way analysis of variance (ANOVA) with post hoc Fisher's LSD test (OriginPro 8.5), and  $P$ -

values  $< 0.05$  were considered statistically significant. The results were deemed significant at  $0.01 < *P \leq 0.05$ , highly significant at  $0.001 < **P \leq 0.01$ , and extremely significant at  $***P \leq 0.001$ .

## 3. Results and discussions

To test if the azido-bearing metabolic sugar precursors can label host cells, we chose RAW264.7 murine macrophages as a model host cell to evaluate the labeling capability of a series of azido-sugars: Ac<sub>4</sub>ManNAz (AAM), ManNAz (AM), Ac<sub>4</sub>GalNAz (AAG) and GalNAz (AG) (Fig. S1a). RAW264.7 macrophages were incubated with the corresponding azido-sugar for 24 h, followed by probing with dibenzocyclooctyne (DBCO)-Cy5. AAG showed the highest labeling efficiency in macrophages among all tested sugars, possibly as a result of the higher abundance and faster uptake rate (Fig. S1b). Azido-glycoprotein analysis by Western blotting confirmed that AAG had the highest labeling efficiency in macrophages. During this process, the azido modified glyco-proteins were first biotinylated by incubating with DBCO-PEG<sub>4</sub>-biotin and then detected by streptavidin-horseradish peroxidase (HRP) conjugate. The results demonstrate that azido labeling occurs on the glycoproteins of the cell surface (Fig. S1c). The "band" appears as a smear because GalNAz can finally appear as both GalNAz or GlcNAz (by the salvage pathway) on the glycoproteome [28], and the polysaccharide chain on the glycoprotein is highly diversified as it was reported previously [29].

We used the structure of AAG for the development of sugar precursors for specifically labeling infection sites. Our previous work has demonstrated that blocking the anomeric position (1') of the azide substituted sugar precursor can greatly inhibit the labeling ability of the sugar [21], which prompted us to design a trigger-responsive sugar for infection-site specific labeling. Thiol-ketal based biomaterials have been developed for the ROS responsive release of therapeutic agents such as anti-cancer or anti-inflammatory siRNA (Fig. 1a) [30,31]. The thiol-ketal linkers are stable under physiological conditions and can be oxidized by ROS to generate hydrophilic ketones and sulfate-containing compounds [32–35]. We reasoned that the hemi-thiol ketal group (Fig. 1a and b) on the anomeric position of AAG can be oxidized by ROS and release the active AAG derivative (Fig. S2) by a similar oxidative mechanism. To prove this hypothesis, we synthesized several Ac<sub>3</sub>GalNAzSP structures. To characterize ROS triggered degradation, Ac<sub>3</sub>GalNAzSP was first incubated in H<sub>2</sub>O<sub>2</sub> solution and then probed with DBCO-Cy5 via Click chemistry to monitor the release of Ac<sub>3</sub>GalNAzOH (AAGOH) by HPLC with a fluorescence detector ( $\lambda_{\text{ext}}$ : 650 nm,  $\lambda_{\text{emi}}$ : 688 nm) (Fig. S3a). The consumption of Ac<sub>3</sub>GalNAzSP and the accumulated release of AAGOH were quantified. The results indicate all three precursors released over 50% after 48 h in oxidative environment. Among them, MBTAAG, a *p*-meoxybenzyl substituted Ac<sub>3</sub>GalNAz sugar precursor showed the highest oxidation responsiveness (Fig. 1c and d). In comparison, no degradation was observed over 48 h under non-oxidative physiological conditions in both PBS and DMEM cell medium supplied with 10% FBS, suggesting minimal release of active labeling agent in normal cells or tissues (Fig. S3b). We also tested the degradation of the MBTAAG precursor in response to biologically relevant levels of H<sub>2</sub>O<sub>2</sub> (e.g. 100  $\mu$ M and 1 mM) [36] by HPLC by coinubation with 100  $\mu$ M MBTAAG. The degradation selectivity of MBTAAG under various ROS signals, including hyperchloride, H<sub>2</sub>O<sub>2</sub>, and hydroxyl radical was also evaluated. This showed that such hemi-thiol ketal linkage showed most efficient degradation in response to the hydroxyl radical (Fig. S4).

To examine the ability of MBTAAG to label host cells under pro-inflammatory conditions, we used lipopolysaccharide (LPS)-activated macrophages to mimic the immune response of macrophages, resulting in a pro-inflammatory response and high ROS levels during the invasion of pathogens [37]. LPS-activated murine macrophages were incubated with MBTAAG, while macrophages treated with PBS and AAG (the labeling active motif of MBTAAG) were used as negative and positive

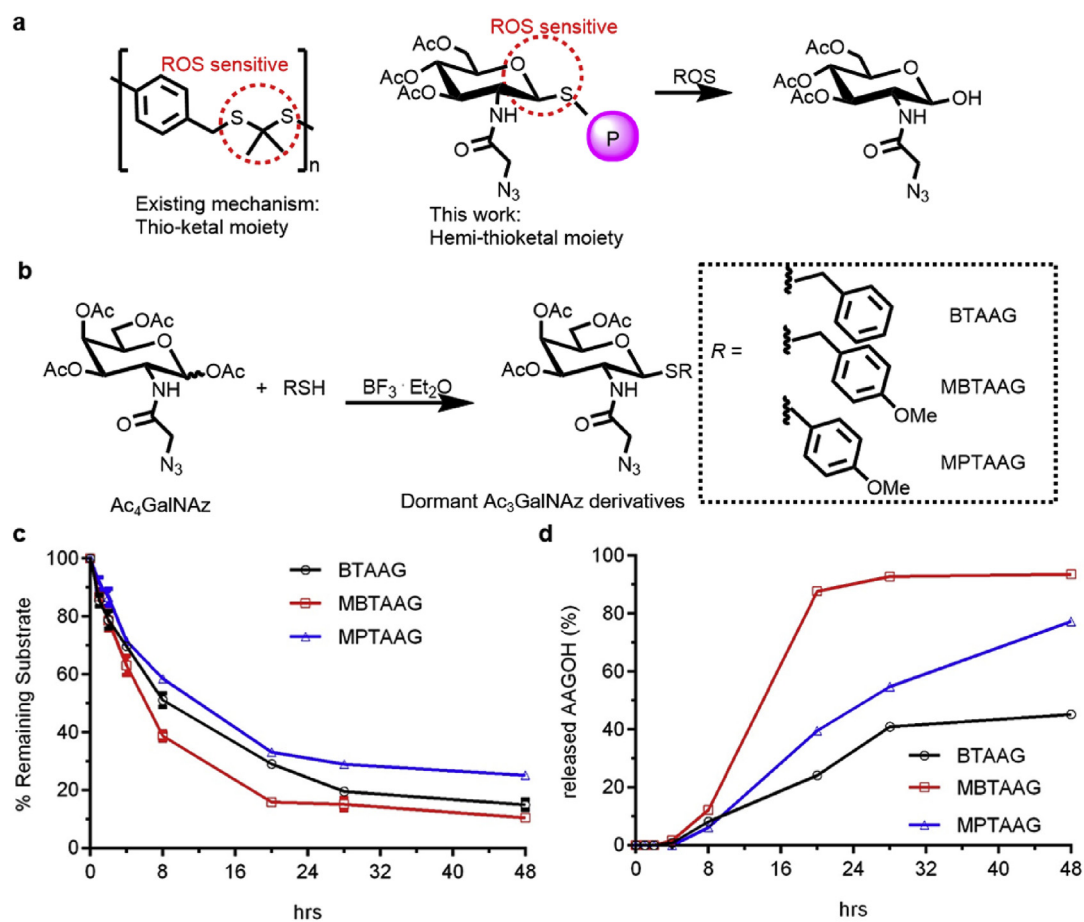


**Fig. 1.** a) Reactive ROS responsiveness of precedent thiol-ketal structure and hemi-thio-ketal structure in this work. b) Brief synthetic route of dormant Ac<sub>3</sub>GalNAz derivatives Ac<sub>3</sub>GalNASP. c) Consumption of Ac<sub>3</sub>GalNAzSP under H<sub>2</sub>O<sub>2</sub>. d) Accumulative release of Ac<sub>3</sub>GalNAzOH (AAGOH) from Ac<sub>3</sub>GalNAzSP under H<sub>2</sub>O<sub>2</sub>. The slightly lagging release of AAGOH as compare to Ac<sub>3</sub>GalNAzSP consumption is due the transformation of intermediates.

controls respectively (Fig. 2a). Treating LPS activated macrophages with MBTAAG resulted in elevated azide expression on cell membranes (Fig. 2b). In contrast, non-activated macrophages cannot be labeled by MBTAAG due to the low ROS levels. AAG, on the contrary, showed very high labeling levels for both LPS-activated macrophages and non-activated macrophages. The marked increase in cellular fluorescence in LPS-induced macrophages treated by MBTAAG was largely mitigated by treating cells simultaneously with ROS scavenger 4-hydroxy-2,2,6,6-tetramethylpiperidine-N-oxyl (TEMPOL) [38], indicating that the increased amount of released AAGOH resulted from elevated intracellular ROS levels. Western blot analysis showed that the elevated labeling of cells overproducing ROS occurred in glycoproteomes (Fig. 2c). Similar results were also demonstrated by flow cytometry analysis (Fig. 2d and e). In a separate study, we tested the level of unspecific MBTAAG labeling in normal epithelial cells with Chinese Hamster Ovary (CHO) cell line. MBTAAG showed negligible labeling in CHO cells (Fig. S5). These results indicate the promising discrimination effect between pro-inflammatory host cells and normal cells for labelling.

We next tested our hypothesis that host cells infected with bacteria could trigger the release of active azido-sugars, presenting azido groups on cell surfaces. We infected RAW264.7 murine macrophages with pathogens *Escherichia coli* (Gram-negative) or *S. aureus* (Gram-positive) at multiplicity of infection (MOI) of 100: 1. Extracellular bacteria were killed by gentamycin, which is uptaken too slowly to kill intracellular pathogens [39]. It is observed that nearly all the host cell population was labeled by MBTAAG, as MBTAAG and AAG showed nearly identical labeling efficiency (Fig. 3a and b). MBTAAG showed very low background labeling for uninfected cells (Fig. 3c and d), and the signal

enhancement was 7.2 times and 6.5 times after infection in *E. Coli* or *s. aureus* infected cells, respectively. To confirm that infected host cells spontaneously generate ROS, we visualized intracellular ROS generation using 2',7'- dichlorofluoresceindiacetate (DCFDA) [40], a cell permeable fluorescent dye that is rapidly oxidized to a fluorescent molecule by intracellular ROS. Confocal microscopy analysis clearly demonstrated the generation of intracellular ROS throughout the cell during the infection (Fig. 3f), and MBTAAG labeling of infected macrophages is well co-localized with ROS positive macrophages, indicating the selective labelling is resulted from overexpressed ROS in infected host cell niche. To test the quantitative correlation between labeling and multiplicity of infection, we infected RAW264.7 murine macrophages with GFP-engineered pathogens *E. coli* (Gram-negative) or *Bacillus subtilis* (Gram-positive) at different multiplicity of infection (MOI) ratios ranging from 1:1 to 100:1. The infected macrophages were incubated with MBTAAG for 12 h and probed by DBCO-Cy5 afterwards. Double channel flow cytometry analysis (GFP and Cy5) revealed that the infected host cells could be labeled by MBTAAG with high specificity (quadrant I compared to quadrant II), while AAG, indiscriminately labeled all populations of macrophages (Fig. 3e and g and S6). Also, the 'double positive' population (GFP<sup>+</sup>, Cy5<sup>+</sup>) was increased when pathogen loading was increased, making it possible to quantify infected cells during *in vitro* studies or in homogenized tissues from animal studies. Incorporation of DBCO-Cy5 dye onto host macrophages was also confirmed by confocal microscopy (Figs. S7a and S7b). MBTAAG can specifically label infected macrophages and shows a good correlation between infected macrophages (Channel Green) and azide labeled macrophages (Channel Red).

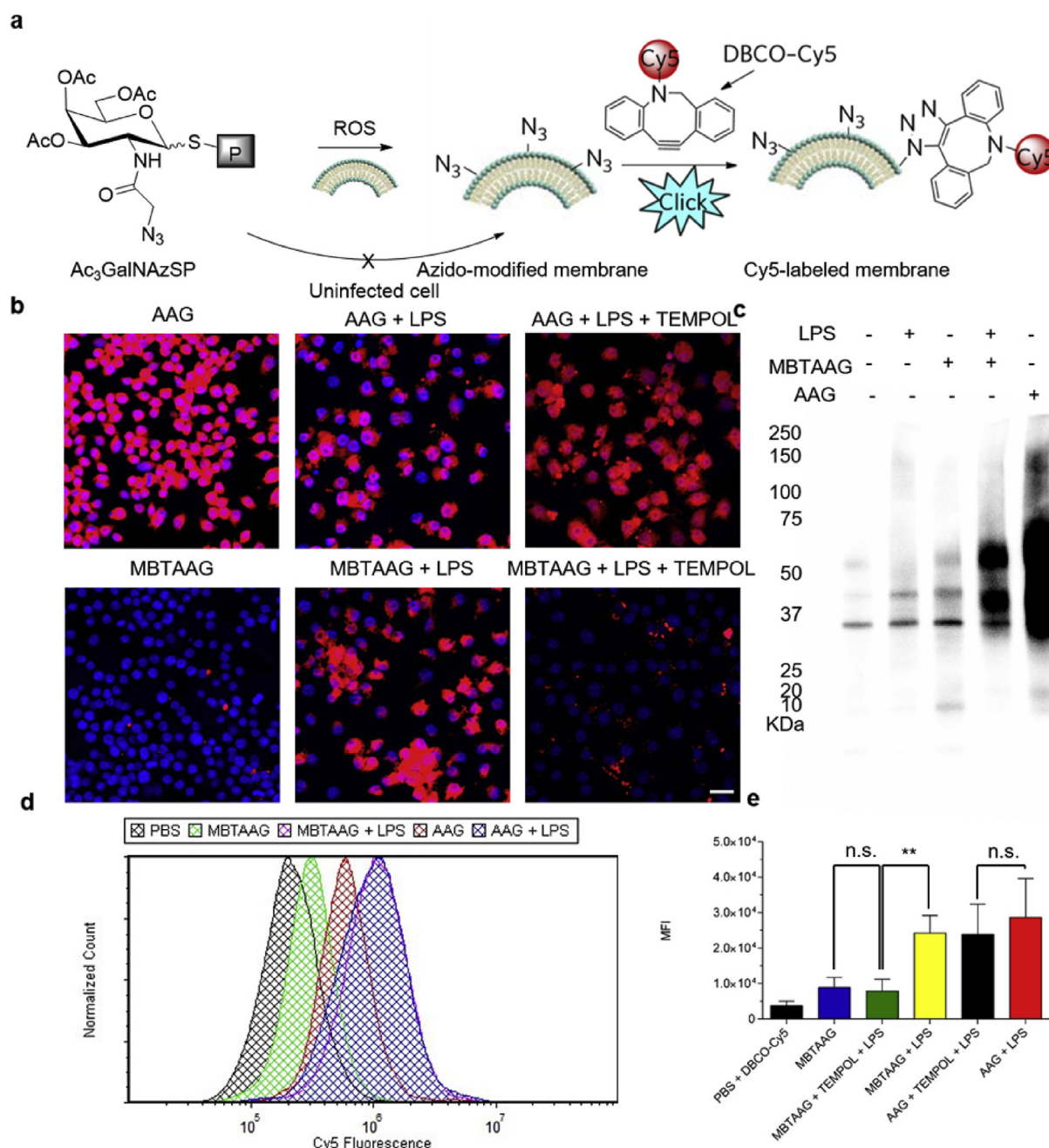


**Fig. 2.** a) Schematic illustration of Reactive Oxygen Species (ROS) activated metabolic labeling of  $Ac_3GalNAzSP$  and subsequent detection of the expressed azido groups by DBCO-Cy5 via copper-free click chemistry. b) Confocal laser scanning microscopy (CLSM) image of RAW264.7 murine macrophage after incubation with  $Ac_3GalNAz$  (AAG) or MBTAAG for 48 h, followed by co-incubation with 5  $\mu g/mL$  LPS (or spike with 5 mM TEMPOL for ROS inhibition) and labeling of DBCO-Cy5 (50  $\mu M$ , red) for 1 h. The cell nuclei were stained with Hoechst 33342 (blue). Scale bar, 50  $\mu m$ . c) Western blotting analysis of RAW264.7 cells after treatment with PBS, MBTAAG, or AAG for 48 h followed by co-incubation with LPS for 24 h for macrophages activation. Azido-modified proteins were biotinylated by incubating with DBCO-PEG<sub>4</sub>-biotin and then detected by streptavidin-horseradish peroxidase conjugate. PBS and PBS + LPS groups showed only two endogenous biotinylated protein bands. d) Flowcytometry analysis of RAW264.7 cells after treatment with PBS, MBTAAG, or AAG for 48 h, followed by co-incubation with LPS for 24 h for macrophages activation, respectively, and labeled with DBCO-Cy5 (20  $\mu M$ ) for 1 h. e) Quantitative analysis of flowcytometry results generated from (d), TEMPOL (5 mM) was spiked in LPS to trap ROS to confirm the ROS trigger release mechanism of MBTAAG in LPS treated macrophages. All numerical data were presented as mean  $\pm$  SEM ( $n = 3$ ) and analyzed by one-way ANOVA (Fisher;  $0.01 < *P \leq 0.05$ ;  $**P \leq 0.01$ ;  $***P \leq 0.001$ ). (For interpretation of the references to colour in this figure legend, the reader is referred to the Web version of this article.)

We then studied the infection selective labeling capability of MBTAAG *in vivo*, enabled by copper-free Click chemistry mediated fluorescent probe targeting. To examine this, BALB/c mice were intramuscularly injected in the right and left thigh muscles, respectively with *E. coli* ( $10^6$  colony-forming units, CFUs) and PBS. It has been shown that the majority of early soft tissue infections and abscesses caused by bacteria contain more than around  $10^7$  CFU  $mL^{-1}$  burden

[41]. The pathogen burdens are approximately those of the early contact dose of pathogens in typical infectious diseases. After 12 h, a single dose of MBTAAG (76.8 mg/kg) was systematically administered into BALB/c mice via tail vein injection. Mice treated with AAG (64.0 mg/kg) or PBS were used as positive and negative controls. The biodistribution of metabolized azido sugar rather than free, unmetabolized azido sugar was studied by previously reported tissue western blotting

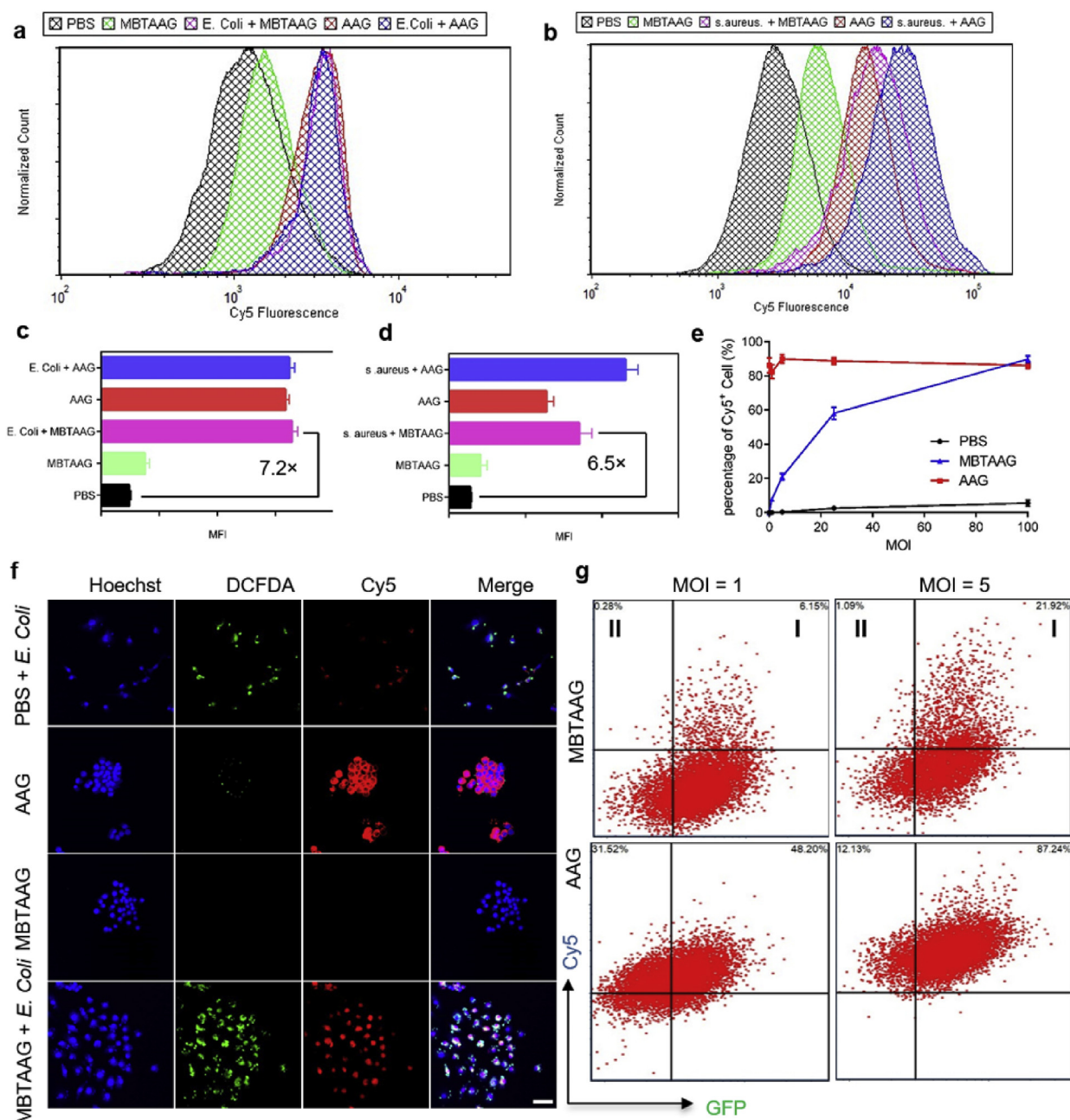


**Fig. 3.** Flow cytometry analysis of RAW264.7 cells after treated with PBS, MBTAAG, AAG for 48 h, followed by co-incubation with gram negative pathogens *E. coli* (a) or gram positive pathogens *S. aureus* (b) when MOI = 100 for 12 h, 2 μg/mL gentamycin was applied to select intracellular pathogens, and labeled with DBCO-Cy5 (20 μM) for 1 h. c,d) Quantitative analysis of mean fluorescence intensity (MFI) derived from FACS result of (a) and (b). e) FACS allows separation of GFP-modified pathogen (*E. Coli*) infected RAW264.7 murine macrophages labeled with MBTAAG in a manner that correlates with the multiplicity of infection (MOI) bacteria per cell. Intracellular bacteria were selected by coinubation with gentamycin (2 μg/mL). Cy5<sup>+</sup> macrophages are defined arbitrarily within the quadrant I and II in (g). f) Generation of intracellular ROS in *E. Coli* infected RAW264.7 murine macrophages was confirmed by DCFDA staining. Strong green fluorescence throughout the cells demonstrates the high level of intracellular ROS in infected RAW264.7 cells and is the cause of MBTAAG labelling of the host macrophages. Cellular nuclei were counterstained with Hoechst 33342 (blue). Scale bar, 50 μm. Nuclei were stained with Hoechst 33342 (blue). Scale bar, 50 μm. All numerical data was presented as mean ± SEM (n = 3). (For interpretation of the references to colour in this figure legend, the reader is referred to the Web version of this article.)

analysis [21]. An increased amount of azido-modified proteins in the MBTAAG group compared to the PBS group was observed 12 h post injection of MBTAAG, while there was a negligible difference observed in the amount of azido-modified proteins in liver, spleen, heart and lung between MBTAAG and PBS groups (Fig. S8). In contrast to those results, AAG showed nonspecific labeling in normal tissues, with a considerable amount of azido groups expressed in liver and kidney. In a separate study, DBCO-Cy5 was then intravenously injected at 12 h post azido-sugar injections, and its biodistribution was monitored through non-

invasive near infrared (NIR) *in vivo* imaging (Fig. 4a). The elevated accumulation of DBCO-Cy5 at infected muscle tissue was observed at early stages, at the time when free fluorophore dominates the fluorescent intensity contribution in systemic circulation (Figs. 4b and 5a). At 12 h post injection of DBCO-Cy5, infected thighs showed much higher accumulation of fluorescent probes than uninfected thighs or PBS treated groups confirmed by noninvasive *in vivo* imaging. The harvested infected thighs of MBTAAG-treated mice showed a Cy5 fluorescence intensity increase of 2.25-fold over that of uninfected

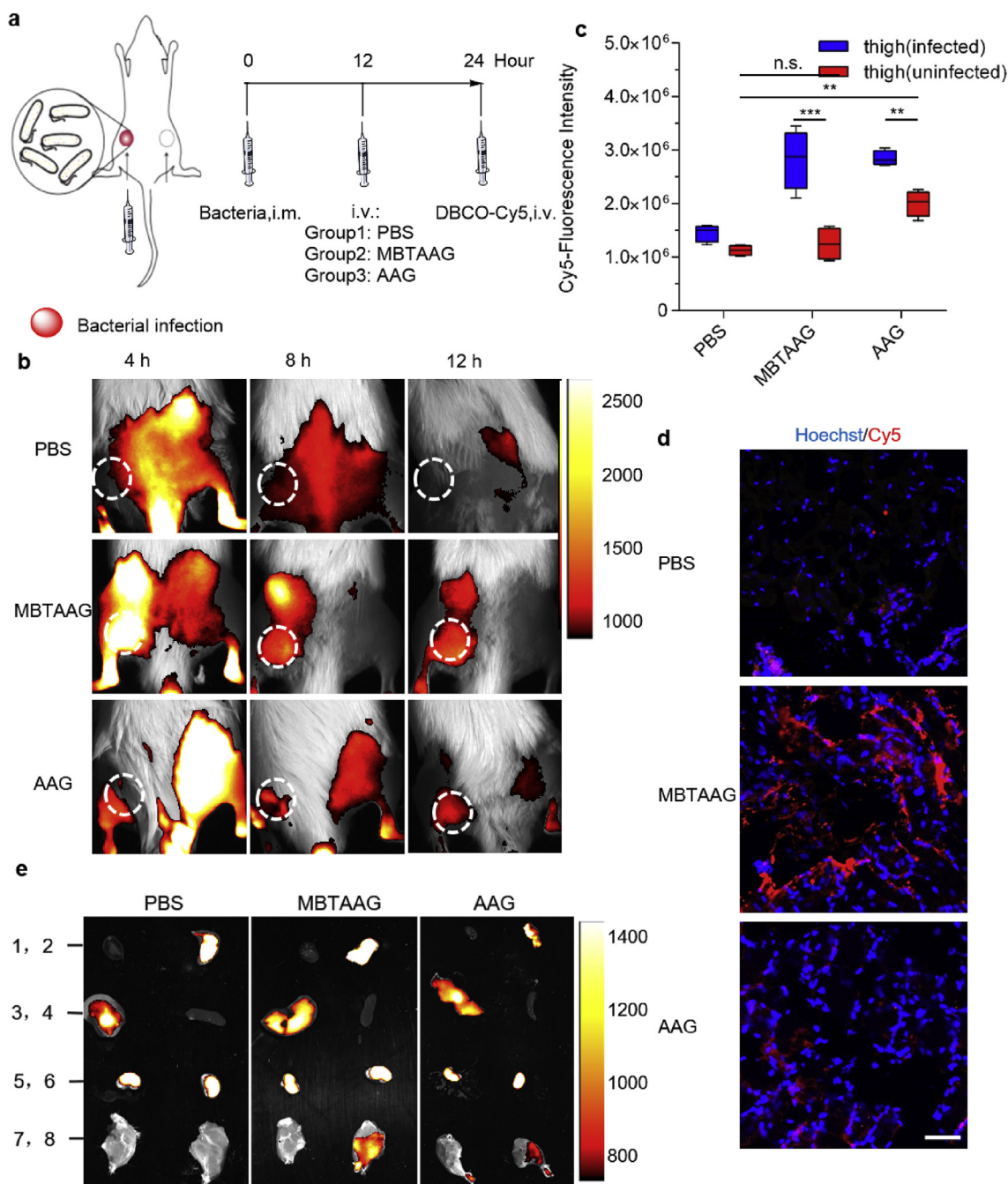


**Fig. 4.** a) Time frame of *in vivo* imaging study. b) *In vivo* whole-body fluorescence imaging of BALB/c mice at 4, 8, 12 h post injection of DBCO-Cy5, respectively. Dot lines indicate the induced myositis area. c) Quantification of Cy5 FI in thigh muscles from (e). d) CLSM images of infected thigh sections from each group. The cell nuclei were stained with Hoechst 33342 (blue). Scale bar, 50  $\mu$ m. e) *Ex vivo* imaging of thigh muscles and major organs at 12 h post injection of DBCO-Cy5. 1-heart, 2-lung, 3-liver, 4-spleen, 5,6-kidneys, 7-right (uninfected) thigh, 8-left (infected) thigh. All numerical data were presented as mean  $\pm$  SEM (n = 8) and analyzed by one-way ANOVA (Fisher; 0.01 < \*P  $\leq$  0.05; \*\*P  $\leq$  0.01; \*\*\*P  $\leq$  0.001). (For interpretation of the references to colour in this figure legend, the reader is referred to the Web version of this article.)

thighs which had the same fluorescence level as the PBS-treated group (Fig. 4c). The localization of Cy5 probe was confirmed by confocal microscopy images of harvested infected tissue (Fig. 4d). On the contrary, the AAG-treated group had similar fluorescence levels in infected tissue compared to the MBTAAG-treated group at the same time and showed nonspecific retention of fluorescent probes in the uninfected tissue and organs such as the liver and kidneys (Figs. 4c and 5b). In contrast, there were no significant differences in Cy5 retention in the liver, spleen, heart, lung and kidney tissues between MBTAAG-treated mice and PBS-treated mice, indicating very low nonspecific labeling of

MBTAAG in normal tissue (Figs. 4e and 5b). To confirm the site-specific labeling is resulted from elevated ROS levels *in vivo*, we utilized ROS responsive indicator L-012 to probe ROS levels [42]. This showed that the labeling of MBTAAG is highly colocalized with elevated ROS levels. At the same time, labeling can be inhibited by administration of TEMPOL at the infection site (Fig. S9). We also stained infected thighs using macrophage specific anti-CD68 antibodies for immunostaining. An obvious correlation of Cy5 (Red) and macrophage fluorescence (CD68, yellow) (Fig. 5c) was observed, indicating that labeling mostly occurred on effector cells that secrete ROS chemokines in response to

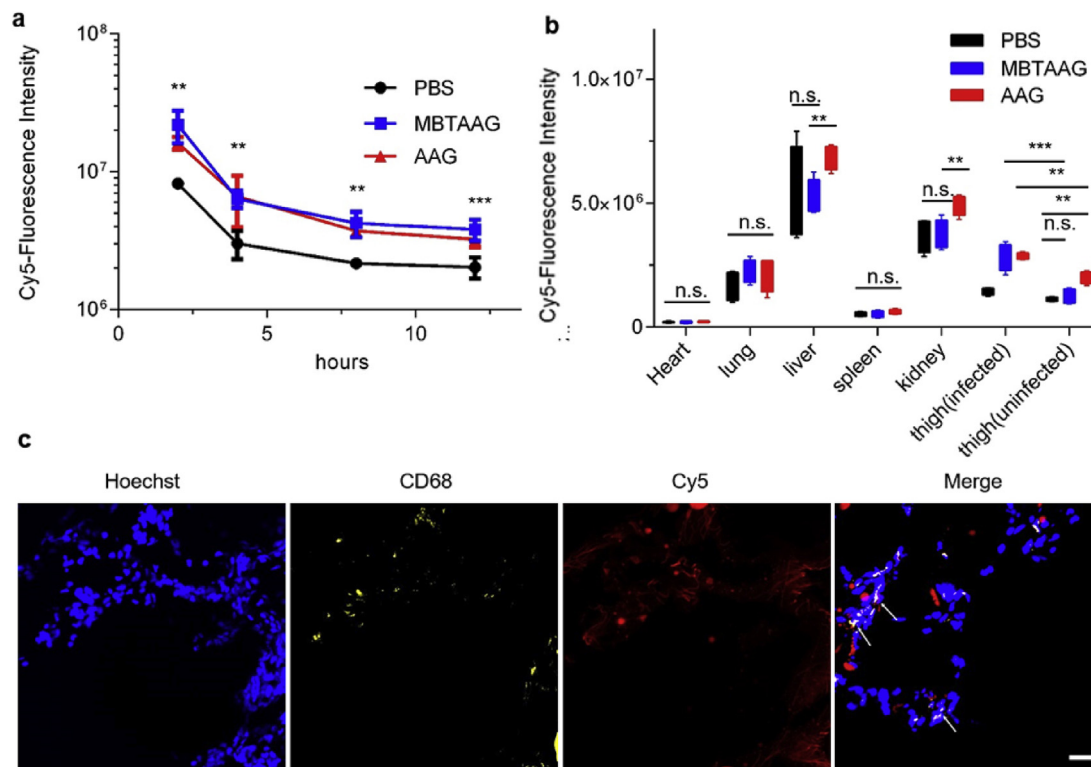


**Fig. 5.** a) DBCO-Cy5 retention kinetics in *in vivo* imaging of infected flank of thigh muscles. Significance test was performed between MBTAAG treated groups and PBS treated groups. b) Mean Cy5 fluorescence intensity of tissues extracted from Fig. 4c. All numerical data was presented as mean ± SEM (n = 8) and analyzed by one-way *t*-test (Fisher; 0.01 < \**P* ≤ 0.05; \*\**P* ≤ 0.01; \*\*\**P* ≤ 0.001). c) Histological analysis of DBCO-Cy5 labeling after one dose treatment of MBTAAG followed by systemic administration of DBCO-Cy5 (Red) in infected thigh tissue. CD68 (yellow) was used as marker for immunofluorescence staining for the recognition of macrophages. Cell nuclei were stained with Hoechst 33342. Scale bar, 50 μm. (For interpretation of the references to colour in this figure legend, the reader is referred to the Web version of this article.)

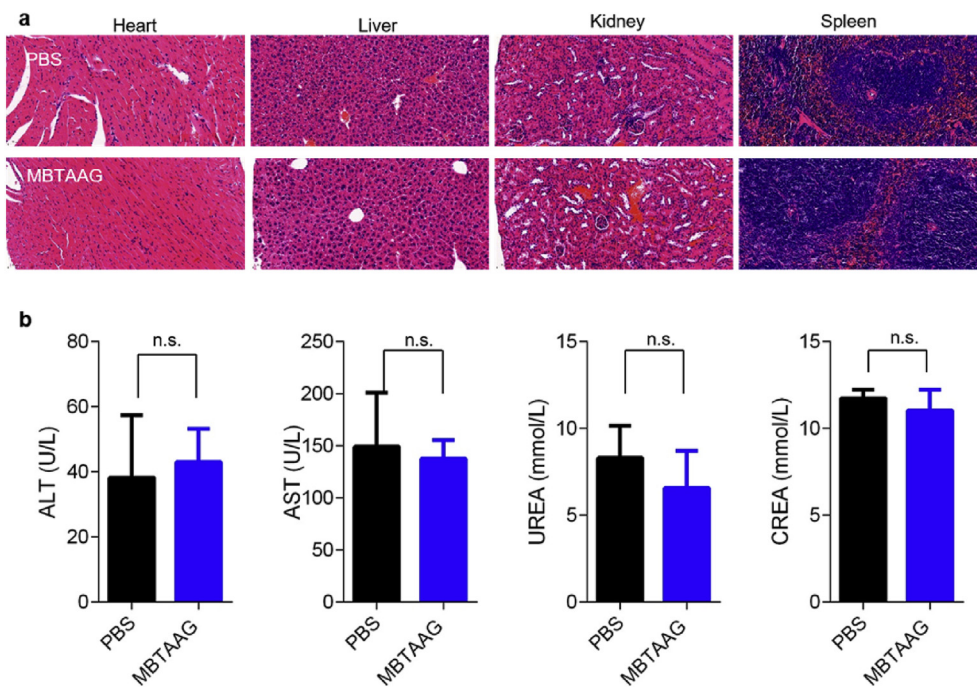


**Fig. 6.** a) Histopathology of mouse tissues following an intravenous injection of MBTAAG. Representative sections of various organs taken from control mice receiving PBS and mice receiving 76.8 mg/kg MBTAAG 48 h post-injection were stained by hematoxylin and eosin. (n = 5 for each group) No organs showed any acute inflammations. b) Acute liver toxicity was also indicated by serum biochemistry index. ALT: Alanine transaminase, AST: Aspartate transaminase, UREA: Blood Urea Nitrogen (BUN), CREA: creatinine. All numerical data was presented as mean ± SEM (n = 5) and analyzed by one-way *t*-test.

invading pathogens. The toxicity of MBTAAG was evaluated both *in vitro* and *in vivo*. The *in vitro* evaluation of MBTAAG showed that it is nontoxic by standard cell viability assay (Fig. S10). The blood biocompatibility of MBTAAG was further evaluated by hemolysis of human red blood cells (Fig. S11), showing the low hemolytic potential of

MBTAAG. This showed HC50 > 5000 μg/mL, which is far higher than the injected concentration *in vivo*. Acute *in vivo* toxicity experiments were performed after *i.v.* administration of 76.8 mg/kg in ICR mice. There was no mortality or deterioration under general conditions observed in mice. Representative sections of various organs taken 48 h

after injections from control mice receiving PBS and mice receiving MBTAAG were stained by hematoxylin and eosin (Fig. 6a). No liver or kidney toxicity was observed by evaluating the serum biochemistry index ALT, AST, Blood Urea Nitrogen (BUN) and creatinine (Fig. 6b). The absence of immune or inflammatory reactions after MBTAAG administration supports the lack of toxicity.

#### 4. Conclusion

Targeting intracellular pathogens has never been achieved by conventional pathogen targeting agents. In this work, we circumvent this by incorporating a selective metabolic labeling technique for infected host cell specific targeting. Specifically, we designed a ROS responsive sugar precursor for selectively labeling host cells invaded by pathogens both *in vitro* and *in vivo*. Such signals reveal the pro-inflammatory status of the infected cells, resulting a transformable target. By using the optical imaging agent DBCO-Cy5, we achieved highly specific ( $P < 0.001$ ), host cell surface targeted imaging of the infection *in vivo* at the early stages. Our azido sugar MBTAAG offers distinct advantages for targeting host cells that engulfed pathogens which cannot be easily achieved by conventional probes. Investigation of host cell selective metabolic labeling followed by treatment with DBCO-antibiotics are currently in progress in our group. This unprecedented host cell labeling technique coupled with efficient Click Chemistry, opens new opportunities for the development of infection responsive sugar precursors for the precise diagnosis and treatment of many infectious diseases.

#### Author information

The manuscript was written through contributions of all authors. All authors have given approval to the final version of the manuscript. The authors declare no competing financial interest.

#### Acknowledgment

This work was supported by National Institute of Health (NIH-1R01EB025651).

#### Appendix A. Supplementary data

Supplementary data to this article can be found online at <https://doi.org/10.1016/j.biomaterials.2020.119843>.

#### References

- [1] Y. Alhamdi, D.R. Neill, S.T. Abrams, H.A. Malak, R. Yahya, R. Barrett-Jolley, et al., Circulating pneumolysin is a potent inducer of cardiac injury during pneumococcal infection, *PLoS Pathog.* 11 (5) (2015) e1004836.
- [2] S. Gagneux, Ecology and evolution of *Mycobacterium tuberculosis*, *Nat. Rev. Microbiol.* 16 (4) (2018) 202.
- [3] J. Libertucci, V.B. Young, The role of the microbiota in infectious diseases, *Nature Microbiology* 4 (1) (2019) 35–45.
- [4] G. Van Cutsem, P. Isaakidis, J. Farley, E. Nardell, G. Volchenkov, H. Cox, Infection control for drug-resistant tuberculosis: early diagnosis and treatment is the key, *Clin. Infect. Dis.* 62 (suppl\_3) (2016) S238–S243.
- [5] J.J. Erasmus, H.P. McAdams, M.A. Farrell, E.F. Patz Jr., Pulmonary nontuberculous mycobacterial infection: radiologic manifestations, *Radiographics* 19 (6) (1999) 1487–1503.
- [6] G. Gao, Y.-W. Jiang, H.-R. Jia, F.-G. Wu, Near-infrared light-controllable on-demand antibiotics release using thermo-sensitive hydrogel-based drug reservoir for combating bacterial infection, *Biomaterials* 188 (2019) 83–95.
- [7] Y. Kong, H. Yao, H. Ren, S. Subbian, S.L. Cirillo, J.C. Sacchetti, et al., Imaging tuberculosis with endogenous  $\beta$ -lactamase reporter enzyme fluorescence in live mice, *Proc. Natl. Acad. Sci. Unit. States Am.* (2010) 201006643.
- [8] X. Ning, S. Lee, Z. Wang, D. Kim, B. Stubblefield, E. Gilbert, et al., Maltodextrin-based imaging probes detect bacteria *in vivo* with high sensitivity and specificity, *Nat. Mater.* 10 (8) (2011) 602.
- [9] M. Van Oosten, T. Schäfer, J.A. Gazendam, K. Ohlsen, E. Tsompanidou, M.C. De Goffau, et al., Real-time *in vivo* imaging of invasive-and biomaterial-associated bacterial infections using fluorescently labelled vancomycin, *Nat. Commun.* 4 (2013) ncomms3584.
- [10] F.J. Hernandez, L. Huang, M.E. Olson, K.M. Powers, L.I. Hernandez, D.K. Meyerholz, et al., Noninvasive imaging of *Staphylococcus aureus* infections with a nuclease-activated probe, *Nat. Med.* 20 (3) (2014) 301.
- [11] P. Panizzi, M. Nahrendorf, J.L. Figueiredo, J. Panizzi, B. Marinelli, Y. Iwamoto, et al., *In vivo* detection of *Staphylococcus aureus* endocarditis by targeting pathogen-specific prothrombin activation, *Nat. Med.* 17 (9) (2011) 1142–1146.
- [12] S.H. Kaufmann, Immunity to intracellular bacteria, *Annu. Rev. Immunol.* 11 (1) (1993) 129–163.
- [13] D.E. Rogers, Studies on bacteremia: I. Mechanisms relating to the persistence of bacteremia in rabbits following the intravenous injection of staphylococci, *J. Exp. Med.* 103 (6) (1956) 713–742.
- [14] S.M. Lehar, T. Pillow, M. Xu, L. Staben, K.K. Kajihara, R. Vandlen, et al., Novel antibody-antibiotic conjugate eliminates intracellular *S. aureus*, *Nature* 527 (7578) (2015) 323.
- [15] M. Fraunholz, B. Sinha, Intracellular *Staphylococcus aureus*: live-in and let die, *Frontiers in cellular and infection microbiology* 2 (2012) 43.
- [16] C. Garzoni, W.L. Kelley, Return of the Trojan horse: intracellular phenotype switching and immune evasion by *Staphylococcus aureus*, *EMBO Mol. Med.* 3 (3) (2011) 115–117.
- [17] S.T. Laughlin, C.R. Bertozzi, Metabolic labeling of glycans with azido sugars and subsequent glycan-profiling and visualization via Staudinger ligation, *Nat. Protoc.* 2 (11) (2007) 2930–2944.
- [18] M.A. Breidenbach, J.E. Gallagher, D.S. King, B.P. Smart, P. Wu, C.R. Bertozzi, Targeted metabolic labeling of yeast N-glycans with unnatural sugars, *Proc. Natl. Acad. Sci. Unit. States Am.* 107 (9) (2010) 3988–3993.
- [19] P. Calabretta, H.L. Hodges, M.B. Kraft, V. Marando, L.L. Kiessling, Bacterial cell wall modification with a glycolipid substrate, *J. Am. Chem. Soc.* 141 (23) (2019) 9262–9272.
- [20] D. Mao, C. Zhang, J. Liu, X. Wang, B. Li, H. Yan, et al., Bio-orthogonal click reaction-enabled highly specific *in situ* cellularization of tissue engineering scaffolds, *Biomaterials* (2019) 119615.
- [21] H. Wang, R. Wang, K. Cai, H. He, Y. Liu, J. Yen, et al., Selective *in vivo* metabolic cell-labeling-mediated cancer targeting, *Nat. Chem. Biol.* 13 (4) (2017) 415–424.
- [22] H. Wang, M. Gauthier, J.R. Kelly, R.J. Miller, M. Xu, W.D. O'Brien Jr. et al., Targeted ultrasound-assisted cancer-selective chemical labeling and subsequent cancer imaging using click chemistry, *Angew Chem. Int. Ed. Engl.* 55 (18) (2016) 5452–5456.
- [23] M.K. Shim, H.Y. Yoon, J.H. Ryu, H. Koo, S. Lee, J.H. Park, et al., Cathepsin B-specific metabolic precursor for *in vivo* tumor-specific fluorescence imaging, *Angew. Chem.* 128 (47) (2016) 14918–14923.
- [24] R. Wang, K. Cai, H. Wang, C. Yin, J. Cheng, Caged metabolic precursor for DT-diaphorase responsive cell labeling, *Chem. Commun.* 54 (38) (2018) 4878–4881.
- [25] H. Wang, Y. Bo, Y. Liu, M. Xu, K. Cai, R. Wang, et al., *In vivo* cancer targeting via glycopolyester nanoparticle mediated metabolic cell labeling followed by click reaction, *Biomaterials* (2019) 119305.
- [26] E. Kim, H. Koo, Biomedical applications of copper-free click chemistry: *in vitro*, *in vivo*, and *ex vivo*, *Chem. Sci.* 10 (34) (2019) 7835–7851.
- [27] A.T. Dharmaraja, Role of reactive oxygen species (ROS) in therapeutics and drug resistance in cancer and bacteria, *J. Med. Chem.* 60 (8) (2017) 3221–3240.
- [28] H. Boyce, I.S. Carrico, A.S. Ganguli, S.-H. Yu, M.J. Hangauer, S.C. Hubbard, et al., Metabolic cross-talk allows labeling of O-linked  $\beta$ -N-acetylglucosamine-modified proteins via the N-acetylgalactosamine salvage pathway, *Proc. Natl. Acad. Sci. Unit. States Am.* 108 (8) (2011) 3141–3146.
- [29] C.F. Teo, L. Wells, Monitoring protein O-linked  $\beta$ -N-acetylglucosamine status via metabolic labeling and copper-free click chemistry, *Anal. Biochem.* 464 (2014) 70–72.
- [30] D.S. Wilson, G. Dalmasso, L. Wang, S.V. Sitaraman, D. Merlin, N. Murthy, Orally delivered thioketal nanoparticles loaded with TNF- $\alpha$ -siRNA target inflammation and inhibit gene expression in the intestines, *Nat. Mater.* 9 (11) (2010) 923.
- [31] M.S. Shim, Y. Xia, A reactive oxygen species (ROS)-responsive polymer for safe, efficient, and targeted gene delivery in cancer cells, *Angew. Chem. Int. Ed.* 52 (27) (2013) 6926–6929.
- [32] A.K. Shukla, M. Verma, K.N. Singh, Superoxide Induced Deprotection of 1, 3-dithiolanes: A Convenient Method of Dedithioacetalization, (2004).
- [33] H. Jin, T. Zhu, X. Huang, M. Sun, H. Li, X. Zhu, et al., ROS-responsive nanoparticles based on amphiphilic hyperbranched polyphosphoester for drug delivery: light-triggered size-reducing and enhanced tumor penetration, *Biomaterials* 211 (2019) 68–80.
- [34] J. Li, C. Sun, W. Tao, Z. Cao, H. Qian, X. Yang, et al., Photoinduced PEG deshielding from ROS-sensitive linkage-bridged block copolymer-based nanocarriers for on-demand drug delivery, *Biomaterials* 170 (2018) 147–155.
- [35] W. Yin, W. Ke, W. Chen, L. Xi, Q. Zhou, J.F. Mukerabigwi, et al., Integrated block copolymer prodrug nanoparticles for combination of tumor oxidative stress amplification and ROS-responsive drug release, *Biomaterials* 195 (2019) 63–74.
- [36] B. Halliwell, M.V. Clement, L.H. Long, Hydrogen peroxide in the human body, *FEBS Lett.* 486 (1) (2000) 10–13.
- [37] E. Mills, B. Kelly, A. Logan, A. Costa, M. Varma, C. Bryant, et al., Repurposing mitochondria from ATP production to ROS generation drives a pro-inflammatory phenotype in macrophages that depends on succinate oxidation by complex II, *Cell* 167 (2) (2016) 457.
- [38] N.V. Vorobjeva, B.V. Pinegin, Effects of the antioxidants Trolox, Tiron and Tempol on neutrophil extracellular trap formation, *Immunobiology* 221 (2) (2016) 208–219.
- [39] J.M. Buyck, S. Lemaire, C. Seral, A. Anantharajah, F. Peyrussou, P.M. Tulkens, et al., Bacterial Persistence, *In Vitro Models for the Study of the Intracellular Activity of Antibiotics*, Springer, 2016, pp. 147–157.

- [40] B. Genty, J.-M. Briantais, N.R. Baker, The relationship between the quantum yield of photosynthetic electron transport and quenching of chlorophyll fluorescence, *Biochim. Biophys. Acta Gen. Subj.* 990 (1) (1989) 87–92.
- [41] C. König, H. Simmen, J. Blaser, Bacterial concentrations in pus and infected peritoneal fluid—implications for bactericidal activity of antibiotics, *J. Antimicrob. Chemother.* 42 (2) (1998) 227–232.
- [42] A. Kielland, T. Blom, K.S. Nandakumar, R. Holmdahl, R. Blomhoff, H. Carlsen, In vivo imaging of reactive oxygen and nitrogen species in inflammation using the luminescent probe L-012, *Free Radic. Biol. Med.* 47 (6) (2009) 760–766.